JAAS

ROYAL SOCIETY OF CHEMISTRY

TECHNICAL NOTE

View Article Online
View Journal | View Issue

Cite this: *J. Anal. At. Spectrom.*, 2023, **38**, 1927

Interference-free electron probe micro-analysis of bromine in halogen-bearing minerals and glasses: high-resolution measurements and quantitative elemental mapping†

Johannes Hammerli * and Scott Boroughs

Received 15th June 2023
Accepted 9th August 2023

DOI: 10.1039/d3ja00198a

rsc.li/jaas

Previous attempts to measure Br in minerals and glasses *via* electron probe micro-analyzers (EPMA) required interference corrections *via* calibration curves in order to account for Al X-ray overlap with the Br L_β X-ray signal. We present a new approach for using EPMA for Br quantification in halogen-bearing minerals and glasses by measuring the interference-free Br K_α X-ray signal (11.909 keV), using a lithium fluoride (LiF) diffracting crystal. A set of Br-doped glasses as well as Cl- and Br-bearing scapolite-group minerals that were previously characterized by SIMS, INAA, LAICPMS, EPMA, and the Noble Gas Method, is compared to new EPMA measurements. Bromine concentrations in the tested samples range from ~10 to ~3500 μg g^{-1} and our study shows that estimated limit of quantifications of ~120 μg g^{-1} Br and ~15 μg g^{-1} of Cl can be reached. In addition, we show that this new approach permits the acquisition of quantitative Cl and Br maps in minerals, which provide high-resolution insights into crustal fluid properties.

Introduction

Halogens (F, Cl, Br, I) are highly reactive elements and key agents for many geological processes. Their importance ranges from impacting the atmosphere and climate *via*, for example, the breakdown of ozone[1] to being important ligands for mass transfer of economically relevant elements, such as base-metals.[2,3] Fluids derived from different halogen-bearing sources, such as seawater, evaporitic lithologies, or residual bittern brines have distinct halogen ratios (*e.g.*, Cl/Br).[4] Furthermore, fluids emitted from magmatic systems also tend to have relatively restricted halogen ratios, which can be distinct from the above-mentioned fluid sources.[5,6] It follows that the determination of halogens and their ratios can be useful to identify fluid sources in crustal processes, which has direct implications for our understanding of, for example, ore-forming processes[7,8] and the complex global halogen cycle.[9–12] In the absence of useful aqueous fluid- and/or melt inclusions, halogen-bearing minerals, such as apatite, amphibole, biotite, sodalite, or scapolite might be used to gain insights into fluid properties and/or sources, especially if halogen partitioning between the fluid and mineral has been constrained, as in the case for the above minerals.[13–16] In addition to bulk analyses, a range of *in situ* methods have been applied to quantify halogens in minerals, which include secondary ion mass spectrometry (SIMS);[17–19] proton induced X-ray emission (PIXE),[20,21] laser ablation inductively coupled plasma mass spectrometry (LAICPMS)[22,23] or electron probe micro-analyzer (EPMA).[24,25] However, many of these approaches involve instruments that are not readily available or are costly to operate, the destruction of sample material (*e.g.*, LAICPMS), and/or come with analytical challenges such as lack of matrix matched standards or signal interferences. The instrument of choice in regards to minimal damage of sample material, high-spatial resolution analytical capabilities, as well as availability and relatively low analytical costs is the EPMA. The measurement of Cl *via* EPMA is not problematic and concentrations in the tens of μg g^{-1} can be quantified. However, the accurate quantification of Br can be difficult as the Br L_β X-ray line sits on the Al peak shoulder (Al K_α X-ray signal).[24] Most geological samples that may contain halogens are typically Al-rich and hence Br quantification *via* EPMA is challenging. However, recent studies[24,25] developed calibration lines that were anchored by Br-free experimental glasses in order to subtract the spectral overlap induced halogen contents. While this approach allows for Br quantification in minerals and glasses, it has been suggested that for each laboratory and instrument type new calibrations need to be established.[25] Reported detection limits *via* this approach are in the range of ~100–300 μg g^{-1} Br.[24,25] In this study we present a new protocol for Br quantification in glasses and minerals by using the Br K_α X-ray signal, which also permits high-resolution quantitative halogen maps of minerals without the need for interference correction.

School of the Environment, Peter Hooper GeoAnalytical Laboratory, Washington State University, Pullman, USA. E-mail: johannes.haemmerli@wsu.edu

† Electronic supplementary information (ESI) available. See DOI: https://doi.org/10.1039/d3ja00198a

Samples

Br-doped glasses

We analyzed Br-doped glasses of andesitic (A-series; A10, A50, A100, A500, A1000) and rhyodacitic (RD-series, RD10, RD50, RD100, RD500, RD5000) compositions, which were synthesized from natural volcanic rocks and for which detailed information can be found in detailed previous study.[26] The analyzed glasses have previously been characterized by a range of different methods including INAA, EPMA, LAICPMS, and SIMS. Reported bromine concentrations in the analyzed glasses range from ~10 μg g^{-1} to 6500 μg g^{-1}.[25,26] Two 1-inch epoxy discs were prepared with each mount containing several chips of the glass samples. The epoxy discs were stepwise polished with a water-based diamond solution from 6 to 1 μm grainsize.

Scapolite-group minerals

The analyzed scapolite samples include SP, BB1, and SY, which have been characterized in detail in previous studies and have been used as primary standard reference material for LAICPMS analysis.[8,10,27,28] Their Br concentrations have been determined by INNA, the Noble Gas Method, and LAICPMS. Scapolite SP contains the lowest Br concentration with 41 ± 3 (2SD) μg g^{-1} Br (Noble Gas Method value), followed by BB1 with 436 ± 33 (2SD) μg g^{-1} Br and SY with 715 ± 64 (2SD) μg g^{-1} Br. Note that these values represent the revised concentrations,[10] which are ~19% lower than reported in the original study.[27] In addition to these three scapolite samples, we analyzed three gemstone quality scapolite crystal (JHSC-1, JHSC-4, and JHSC-2), which were purchased from online vendors. All these scapolite samples were prepared in the same way as the glass samples. To test the feasibility of quantitative Cl and Br elemental mapping we chose a scapolite grain (sample 22JH-03) in a polished thin section from a biotite-rich schist from the Mesoproterozoic Lemhi sub-basin, Idaho, USA.

Experimental set-up

EPMA quantitative analysis

Due to an essentially unresolvable interference of Al K_α on Br L_α, previous attempts to measure Br in aluminum bearing minerals, involves measuring the Br L_β X-ray line on a thallium acid phthalate (TAP) diffracting crystal and subsequently correcting for the overlap of Al K_β and/or Al K_α on the measured intensity using interference corrections or calibration curves constructed with Br free material, which contain a range of Al concentrations. Though a viable strategy, the relatively low count rates for Br L_β and large magnitude intensity corrections introduce additional measurement uncertainty and increase detection limits.[24,25]

Here, we instead chose to measure the Br K_α X-ray line (11.909 keV), using a lithium fluoride (LiF) diffracting crystal, which is not subject to any significant interferences from major elements in normal silicate matrices. Due to the high excitation energy, this measurement requires a relatively high accelerating voltage, which increases beam damage, time dependent intensity issues, and analytical volume.

EPMA measurements were conducted using the JEOL 8500F Hyperprobe at the Washington State University Peter Hooper GeoAnalytical Laboratory. Data were acquired and reduced using the Probe for EPMA (PFE) software package. In order to maximize on peak count time, and avoid complications due to background interferences, mean atomic number (MAN) background estimates were used.[29]

EPMA spot analyses

Due to the necessity of using a high accelerating voltage (25 kV) for Br K_α, and subsequent potential for analytical artifacts due to beam damage, analyses were conducted in multiple passes with different operating conditions, then combined into a single analysis using PFE. Major and minor elements, with the exception of Al, were acquired at 15 kV and 15 nA, while Br, Cl, S, and Al were acquired at 25 kV and 80 nA (see Table 1 for analytical parameters). If needed, one can also move the analysis location a small amount for each pass to provide a fresh surface in order to further reduce beam damage artifacts, though this obviously comes at the expense of spatial resolution. Depending on spectrometer configuration, multiple passes may also reduce the overall analysis time, if each setup is run for all spots before moving to the next setup, as spectrometer movements will only occur once per setup.

In order to maximize counting statistics for lower detection limits, Br was measured on two spectrometers, and intensities were aggregated using PFE. Due to spectrometer/crystal geometry, Br K_α is at an *L*-value of ~72.3 mm, which is near the minimum travel of most spectrometer types, and therefore cannot be measured on H-type spectrometers, and may require MAN backgrounds for measurement on *L*-type spectrometers, as the low off-peak background position may be too close to the spectrometer limit.

When operating at high currents and long dwell times, time dependent intensity[30] (TDI) should be monitored for all elements and corrected for if necessary. For this study, TDI was generally not significant for scapolite analyses, but depending on the element of interest, it was moderate to severe for the glass analyses and in such cases, TDI was corrected for *via* the PFE software (see Results and discussion section). It should also be noted that TDI intervals should be chosen carefully for trace elements, as poor counting statistics from low count rates can result in poor TDI correction fitment. Intervals should be as long as possible, while still providing enough points for good curve fitting.

For trace element analysis accuracy, particularly when using MAN backgrounds, matrix corrections are critical, and therefore major and minor element compositions must be accurate and comprehensive, even for unanalyzed elements. Probe for EPMA allows for specifying/calculating the concentrations of unanalyzed elements (*e.g.* H, C, and O),

Table 1 EPMA set up for quantitative spot analysis

Element	Si	Ti	Al	Fe[a]	Mn[a]	Mg	Ca	Na	K	P	S	Br[a]	Cl
Crystal	TAP	PETH	TAP	LiF	LiF	TAP	PET	TAP	PET	PETH	PET	LiF	PETH
Count time (s)	30	30	30	30 × 2	30 × 2	30	30	30	30	30	60	480 × 2	480
Voltage (kV)	15	15	25	15	15	15	15	15	15	15	25	25	25
Current (nA)	15	15	80	15	15	15	15	15	15	15	80	80	80
~Detection limit (μg g^{-1})	90	60	35	175	180	75	130	120	130	60	40	35	4
Standard	Wollastonite	Rutile	K-412	Hematite	MnF2	K-412	K-412	Albite	KBr	Cl-apatite	Anhydrite	KBr	Cl-apatite

[a] Denotes that the respective element was measured on two crystals simultaneously.

which can have a significant effect on the final calculated concentrations when not accounted for.

The limit of detection (LOD) is calculated at the 99% confidence level, which corresponds to a peak count that is three times higher than the standard deviation of the mean background count by also applying ZAF corrections to account for the sample matrix. We define the estimated limit of quantification (LOQ) for EPMA measurements as the tenfold standard deviation of the mean background. It follows that the limit of detection with our set up is ~35 μg g^{-1} for Br and ~4 μg g^{-1} for Cl and the estimated limit of quantification is ~120 μg g^{-1} for Br and ~15 μg g^{-1} for Cl.

EPMA quantitative elemental maps

A scapolite grain from a biotite-rich schist from the Mesoproterozoic Lemhi sub-basin, ID, USA, was used to assess the feasibility of quantitative mapping for Br and Cl. Maps were acquired using ProbeImage and concentrations were calculated using CalcImage (**probesoftware.com**). CalcImage uses a Probe for EPMA sample setup and spot analyses on standards to apply calibration standards and matrix/interference corrections to each pixel of the map, the same as a conventional spot analysis.[31] Since an accurate matrix correction is essential, major elements should be acquired or, if accurate stoichiometric relationships apply, they can be specified. For this scapolite, CO_2 was specified as the remaining constituent by subtracting the analytical total from 100%, and O was specified by stoichiometry. Two passes were used to acquire Si, Al, Ca, K, Na, Fe, Cl, and Br. Pixel dwell times were 1.85 seconds for Cl, Br, and Al, while Si, Ca, K, Na, and Fe were acquired with a 0.2 second dwell time with a pixel dimension of 5 × 5 μm. With this setup, detection limits for elements acquired with a 0.2 second dwell time were 525–1600 μg g^{-1}, and elements acquired with a 1.85 second dwell time were 80–500 μg g^{-1} (Table 2).

LAICPMS Cl/Br and trace element analysis

Synthetic glasses and scapolite minerals were analyzed at the Radiogenic Isotope and Geochronology Lab (RIGL) at Washington State University using an Analyte G2 193 excimer laser ablation system coupled with a Thermo-Finnigan Element 2 single-collector, inductively coupled, plasma mass spectrometer. We applied a 40 μm-diameter laser spot size with a 10 Hz repetition rate and a laser fluence of ~5 J cm^{-2}. A 15-second blank measurement of the He and Ar carrier gasses (laser off) was collected before each analysis followed by scans across masses in low-resolution mode of an extended element list: ^{29}Si, ^{35}Cl, ^{43}Ca, ^{79}Br, ^{81}Br, ^{89}Y, ^{140}Ce, ^{141}Pr, ^{146}Nd, ^{147}Sm, ^{151}Eu, ^{157}Gd, ^{159}Tb, ^{163}Dy, ^{165}Ho, ^{166}Er, ^{169}Tm, ^{172}Yb, ^{175}Lu during ~30 seconds laser ablation period. Sample time for Cl and Br was set at 100 ms and Sm and Nd peaks were sampled for 30 ms. All other elements were sampled for 20 ms. Trace elements are not further discussed in this study; however, all data can be found in the ESI tables.† Analyses of scapolite or glass unknowns were interspersed with analyses of external calibration standards, typically with 10–12 unknowns bracketed by multiple analyses of three different scapolite standards (BB1, SY, SP) and NIST610 and NIST612 glasses. Scapolite BB1 or SY[10,27,28] was used to standardize Cl and Br, and the NIST610 standard[32] was used for standardization of trace elements while NIST612 was used a secondary standard to monitor analytical performance. For all measurements SiO_2 determined by EPMA was used as the internal standard. Data were processed offline

Table 2 EPMA set up for quantitative elemental mapping

Element	Si	Al	Fe	Ca	Na	K	Br[a]	Cl[a]
Crystal	PET	TAP	LiF	LiF	TAP	PETH	LiF	PETH
Dwell time (s)	0.2	1.85	0.2	0.2	0.2	0.2	1.85 × 2	1.85 × 2
Voltage (kV)	15	25	15	15	15	15	25	25
Current (nA)	60	100	60	60	60	60	100	100
~Detection limit (μg g^{-1})	525	135	1600	1300	700	275	500	80
Standard	K-412	K-412	K-412	K-412	Albite	KBr	KBr	Cl-apatite

[a] Denotes that the respective element was measured on two crystals simultaneously (see main text).

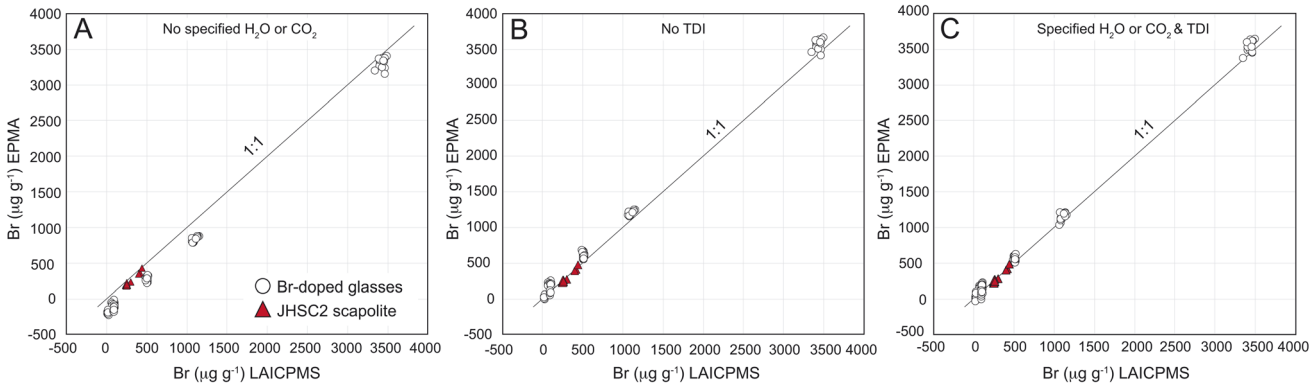

Fig. 1 Comparison of Br contents determined by LAICPMS and EPMA. EPMA data were reduced (A) without specifying H_2O or CO_2, (B) specifying H_2O or CO_2 but with no TDI correction, and (C) with a combination of specified H_2O or CO_2 and TDI correction. Glasses are shown as round symbols and scapolite JHSC2 analyses are shown as red triangle symbols.

using the Iolite 4 software package[33] and detection limits were calculated according to the Pettke reduction scheme[34] and were typically in the range of 7 to 10 μg g^{-1} for Br and 100 to 250 μg g^{-1} for Cl. As described in previous studies[22] we noticed an interference on the mass 35 (chlorine) peak during the ablation of Cl-absent minerals, such as Cl-devoid plagioclase. It is unclear what exactly causes the interference, however, previous studies proposed that "contamination" released from the ablation chamber might cause this interference when material is ablated.[22] Our data show that a signal of ~4800 cps Cl is produced when Cl-free plagioclase is analyzed. By accounting for the fraction of "false" Cl cps, the Cl signal of the unknowns can be corrected for. While the exact cause of the interference on the mass 35 signal is outside the scope of this paper, for minerals (and glasses) with elevated Cl contents (*i.e.*, wt% levels), these "false" Cl signals are typically within the analytical uncertainty.

Results and discussion

Effects of specifying H_2O and CO_2 and TDI corrections for EPMA data reduction

The effects of specifying the volatiles H_2O and CO_2 as well as applying TDI corrections was tested during EPMA data reduction. Fig. 1 compares Br quantified by LAICPMS with Br determined by EPMA when reduced with non-specified H_2O and CO_2 (Fig. 1A), no TDI correction (Fig. 1B), and data reduced when H_2O and CO_2 is specified and TDI is corrected for (Fig. 1C). Fig. 1A shows that specifying H_2O and CO_2 is critical in cases where these components are abundant (*i.e.*, at weight% concentrations). No specified H_2O in glasses (all glasses contain between 3.8 and 6.5 wt% H_2O[26]) results in significantly underestimated Br concentrations. As shown *via* scapolite sample JHSC2, which contains ~1.2 wt% CO_2 (shown as red triangles in Fig. 1), the effect of non-specified CO_2 is less pronounced in this case, yet Br concentrations determined by EPMA also plot below the 1 : 1 line. EPMA data reduced without

Table 3 Mean values of Br and Cl of the analyzed scapolite minerals[a]

	Kendrick *et al.*[10] (2013)	Hammerli *et al.*[23] (2013)	This study	This study
Method	Noble Gas Method	LA-ICP-MS	LA-ICP-MS	EPMA
Spot size	N/A	60 μm	40 μm	10 μm
Sample	**Br (μg g^{-1})**			
BB1	436 ± 33	432 ± 33	446 ± 27 (n = 21)	408 ± 45 (n = 22)
SY	715 ± 64	690 ± 54	731 ± 22 (n = 12)	721 ± 75 (n = 54)
SP	41 ± 3	41 ± 6	48 ± 5 (n = 29)	34 ± 67 (n = 45)
JHSC1			352 ± 16 (n = 18)	341 ± 30 (n = 23)
JHSC2*			252 ± 12 (n = 25)	238 ± 37 (n = 12)
JHSC4			1436 ± 45 (n = 26)	1447 ± 79 (n = 115)
Sample	**Cl (wt%)**			
BB1	3.10 ± 0.10	3.07 ± 0.17	3.10 ± 0.19 (n = 21)	3.02 ± 0.14 (n = 22)
SY	3.50 ± 0.20	3.40 ± 0.17	3.48 ± 0.05 (n = 12)	3.50 ± 0.15 (n = 54)
SP	4.00 ± 0.10	3.94 ± 0.25	4.50 ± 0.32 (n = 29)	4.08 ± 0.15 (n = 45)
JHSC1			3.06 ± 0.26 (n = 18)	2.84 ± 0.13 (n = 23)
JHSC2*			2.98 ± 0.18 (n = 25)	2.75 ± 0.17 (n = 12)
JHSC4			2.44 ± 0.13 (n = 26)	2.27 ± 0.05 (n = 115)

[a] All uncertainties are shown as 2SD. Note that only analyses of the homogeneous core of sample JHSC2 are considered in this table.

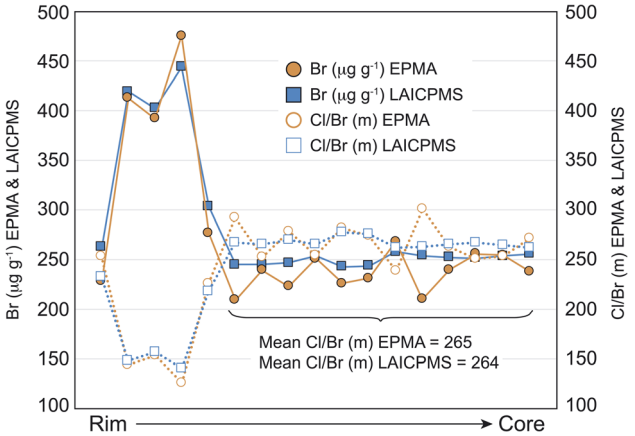

Fig. 2 Comparison of Br concentrations (μg g^{-1}) measured by EPMA and LAICPMS in a compositionally zoned scapolite (JHSC2) and corresponding molar Cl/Br ratios. The *X*-axis shows the transect from the grain's rim to core.

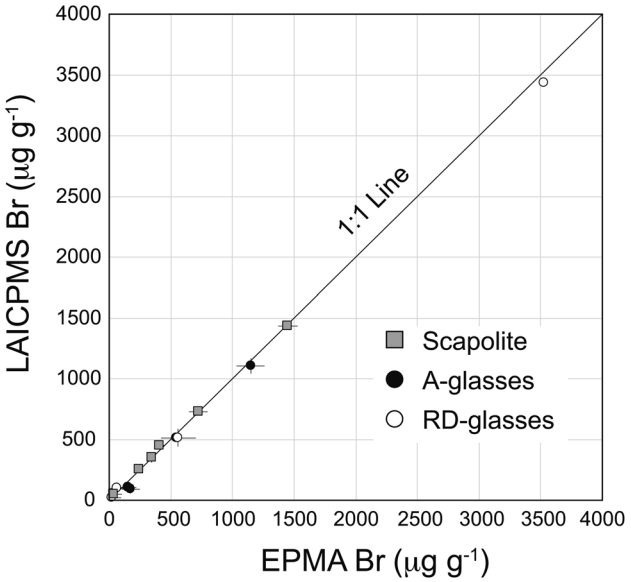

Fig. 3 Comparison of average Br concentrations measured by EPMA and LAICPMS of scapolite minerals (grey squares), A-glasses (black circles), and RD-glasses (white circles). Uncertainties of means are shown as 2SD.

accounting for TDI (Fig. 1B) (but specified H_2O and CO_2) agree well with LAICPMS data, however, specified H_2O and CO_2 in combination with TDI correction returned the most accurate EPMA values when compared with LAICPMS results (Fig. 1C).

Spot analysis of Br-doped glasses and scapolite minerals

Chlorine and Br concentrations in scapolite determined by EPMA and LAICPMS are in good agreement with previously reported data generated *via* the Noble Gas Method and LAICPMS (Table 3). The uncertainty of the Br concentration in SP scapolite measured by EPMA is relatively large owing to its low Br content, which is close to the LOD of the EPMA method (~35 μg g^{-1}). Samples JHSC1, JHSC2, and JHSC4 have not been characterized previously, however, transects across JHSC1 and JHSC4 show that these grains are homogeneous in respect of their Cl and Br composition. The Br content in JHSC1 measured *via* EPMA (341 ± 31 μg g^{-1}) is in excellent agreement with the LAICPMS results (352 ± 16 μg g^{-1}). JHSC4 scapolite contains an EPMA determined Br concentration of 1447 ± 79 μg g^{-1} that agrees with 1436 ± 45 μg g^{-1} measured by LAICPMS. Scapolite JHSC2 contains a homogeneous inner core but is compositionally zoned in its outer zones. EPMA and LAICPMS analyses along the same transect returned near identical Cl and Br compositions and calculated Cl/Br (*m*) values of the core are in excellent agreement (Fig. 2). The slightly larger variability of Br concentrations detected by EPMA may be due to the method's higher spatial resolution

Table 4 Comparison of Br and Cl contents measured in this study with previously reported values of the same samples[a]

	Cadoux *et al.*[26] (2017)	Cadoux *et al.*[26] (2017)	Cadoux *et al.*[26] (2017)	Flemetakis *et al.*[25] (2020)	This study	This study	This study	This study
Method	INNA	LA-ICP-MS	SIMS	EPMA	LA-ICP-MS	EPMA	LA-ICP-MS	EPMA
Spot size	N/A	90 μm	20 μm	10–20 μm	40 μm	10 μm	40 μm	10 μm
	Br (μg g^{-1})	**Br (μg g^{-1})**	**Br (μg g^{-1})**	**Br (μg g^{-1})**	**Br (μg g^{-1})**	**Br (μg g^{-1})**	**Cl[b] (μg g^{-1})**	**Cl (μg g^{-1})**
A10	9.9 ± 4		14.4 ± 1.4 (n = 15)		16 ± 2 (n = 14)		864 ± 76	701 ± 7
A50	51.3 ± 2		85.8 ± 4 (n = 10)		81 ± 26 (n = 21)	171 ± 72 (n = 21)	856 ± 81	702 ± 10
A100	90.3 ± 6	136	138 ± 13 (n = 15)		101 ± 9 (n = 25)	148 ± 73 (n = 25)	809 ± 118	694 ± 14
A500	524 ± 3.2	423 ± 22	410 ± 13 (n = 10)	409 ± 42	510 ± 15 (n = 18)	545 ± 54 (n = 18)	822 ± 81	698 ± 26
A1000	990 ± 6.4	1102 ± 384	1127 ± 118 (n = 10)	1030 ± 163	1114 ± 66 (n = 18)	1145 ± 56 (n = 113)	825 ± 74	701 ± 7
RD10	8.9 ± 6		4 ± 1 (n = 14)		9 ± 2 (n = 13)		840 ± 97	766 ± 79
RD50	51 ± 14		19 ± 1 (n = 10)		24 ± 6 (n = 25)	16 ± 78 (n = 25)	936 ± 107	860 ± 48
RD100	104 ± 10	119	153 ± 3 (n = 5)		99 ± 6 (n = 13)	61 ± 77 (n = 13)	938 ± 125	834 ± 24
RD500	496 ± 2.8	483 ± 16	614 ± 57 (n = 18)		515 ± 15 (n = 13)	556 ± 76 (n = 13)	889 ± 118	847 ± 7
RD5000	5030 ± 17.4	5355 ± 1270	5287 ± 597 (n = 6)	6512 ± 204	3448 ± 72 (n = 24)	3528 ± 142 (n = 24)	946 ± 148	844 ± 16

[a] Note all uncertainties are 2SD. 2SD and mean values are taken from the ESI of the original study.[26] Number of analyses for Cl *via* EPMA and LAICPMS are equivalent to the number of Br analyses in our study. [b] Corrected for interference on Cl signal.

(spot size 10 μm) and therefore the sampling of more subtle compositional zones compared to LAICPMS measurements conducted with a 40 μm spot.

Our EPMA measurements of glasses with low Br concentrations ≤100 μg g^{-1} show large uncertainties and mean values are mostly in poor agreement with Br contents determined by other methods (Table 4). The estimated limit of quantification for Br is ~120 μg g^{-1} (see above) and hence, EPMA measurements of samples with ≤100 μg g^{-1} Br contents may not return accurate Br concentrations. Furthermore, previous characterizations of the Br-doped glasses show that differences between analytical methods exist. Some glasses contain internal heterogeneities, such as glass A50, for which LAICPMS analyses returned different compositions depending on the spot location, which is reflected by the large uncertainties of the mean values (Table 4). EPMA analyses of Br-doped glasses with ≥500 μg g^{-1} Br agree with our LAICPMS measurements and other analytical methods, with the exception of RD5000 for which both our LAICPMS and EPMA measurements returned significantly lower Br contents (~3500 μg g^{-1}) compared to analyses carried out in previous studies (Table 4 and Fig. 3). It is possible that different fragments of the glass contain different Br contents (*i.e.*, glass has a heterogeneous Br distribution) as a previous study[25] reported significantly higher Br contents (~6500 μg g^{-1}) than reported in the original study.[26] The mean value of our measurements and the concentration of 6500 μg g^{-1} as reported previously,[25] is ~5000 μg g^{-1} Br, which agrees with the INAA measurement (Table 4).

Quantitative elemental mapping

Interference-free Br (and Cl) measurements in minerals and glasses by EPMA permit high-resolution quantitative elemental mapping of these elements in tandem with other major and minor elements. Fig. 4 shows an example of a scapolite in a biotite matrix from the Mesoproterozoic Lemhi sub-basin, Idaho, USA. Elemental maps show that the imaged scapolite grain contains several distinct compositional zones with large variation in Br contents. Some of these zones are only a few μm thin and hence quantification of Cl and Br by LAICPMS would be difficult. In these thin ring-like zones Br contents reach ~9000 μg g^{-1} whereas the outermost zone contains the lowest Br contents (~300 μg g^{-1}) as determined by spot analyses (see ESI†). Chlorine concentrations on the other hand vary significantly less (~1.6 to ~2.6 wt%) and the Cl/Br map (shown as molar ratios (*m*)) reflects the highly variable Br and relatively homogeneous Cl concentrations as distinct zones. High-resolution Cl/Br maps are a powerful tool for identifying fluid sources in the crust, especially when halogen distribution coefficients are known.[14] In the studied example the extremely low Cl/Br (*m*) values (≪647) of scapolite suggest that residual bittern brine fluids were present during its formation. Such fluids can form when halite crystallizes, for example *via* the evaporation of seawater (molar Cl/Br ratio ~ 647), and due to its incompatibility, Br is concentrated in residual bittern brine fluids.[4] The concentric zoning of Br-enrichments in the imaged grain suggests that several pulses of residual saline Br-rich fluid

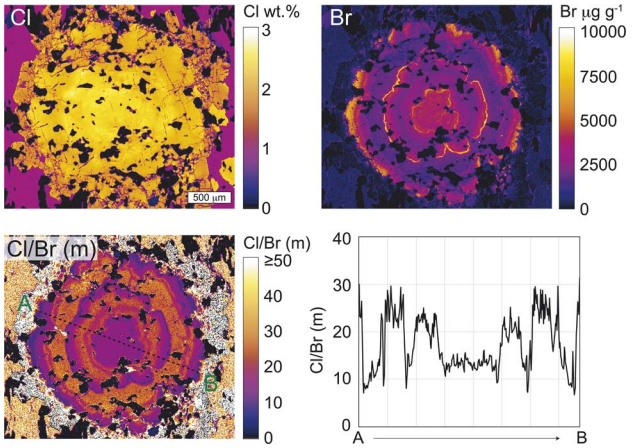

Fig. 4 Quantitative Cl and Br maps of a scapolite grain in biotite-rich schist. Chlorine concentrations show subtle zoning ranging from ~1.6 to ~2.6 wt%. Bromine shows distinct zones reaching 9000 μg g^{-1} in thin concentric rims. Calculated Cl/Br (*m*) ratios show distinct zoning, which follows the Br zonation. A Cl/Br (*m*) transect through high Br zone of the mapped grain shows extremely low Cl/Br (*m*) ratios suggesting the presence of dense residual bittern brine (see main text).

interacted with this rock unit during metamorphism, followed by a fluid with a slightly higher Cl/Br (*m*) ratio (~100–200) as reflected in the mineral grain's outermost zone, which is however, still significantly lower than seawater and still contains a strong residual bittern brine fluid signature. The identification of fluid sources during fluid–rock interaction is critical to understand mass transfer, for example, in mineralized systems. Scapolite-bearing lithologies are often associated with mineralized systems[8,14,28] and hence EPMA spot analysis and elemental maps can provide high-resolution insights in processes related to ore genesis, such as distinguishing between magmatic-derived ore-forming fluids and ore-bearing fluids with a sedimentary/metamorphic origin.[5,7,8,14,35]

Conclusions

Br contents in minerals and glasses can be quantified *via* EPMA by using the interference-free Br K_α X-ray signal (Fig. 3). With our experimental set up, the estimated limit of quantification is ~120 μg g^{-1} for Br and ~15 μg g^{-1} for Cl. No matrix-matched standardization is required with this approach, however, the specification of H_2O and CO_2 in volatile-bearing minerals is important, which can be done stoichiometrically *via* EPMA analysis for most minerals.[36] Minerals or glasses, such as those characterized in this and previous studies, with known Br contents can be used to check instrument performance and a limited amount of JHSC1 and JHC4 is available for distribution by the authors. In addition to the fact that there is no matrix-matched standardization required, the advantages of EPMA Br quantification over other micro-analytical approaches is its high spatial resolution (≤10 μm), its non-destructiveness, and that EPMA instruments are readily available and relatively cost-effective compared to other methods. The approach described in this study can be a useful tool for experimental

work such as studies conducted to determine Br solubility in magmas and/or partitioning between aqueous fluids and melts;[21,26,37] experiments that help to better constrain the global Br cycle and especially Br degassing in volcanic systems, which directly impacts the composition of the atmosphere. Furthermore, high resolution spot analysis and quantitative Cl/Br mapping can be used to identify and trace fluids in the crust, specifically in mineralized systems where, for example, scapolite-group minerals are commonly present.[8,14,28,38–40]

Conflicts of interest

There are no conflicts to declare.

Acknowledgements

We thank Anita Cadoux for sharing Br-doped glasses and Charles Knaack for preparing the KBr standard. This work was supported by Swiss National Science Foundation grant PZ00P2_180095 to J. H. Thoughtful reviews by two anonymous reviewers improved the manuscript and Emma Stephen is thanked for the editorial handling of this manuscript.

References

1 H. Svensen, N. Schmidbauer, M. Roscher, F. Stordal and S. Planke, *Environ. Chem.*, 2009, **6**, 466.
2 B. W. Yardley, *Econ. Geol.*, 2005, **100**, 613–632.
3 J. J. Hemley, G. L. Cygan, J. B. Fein, G. R. Robinson and W. M. d'Angelo, *Econ. Geol.*, 1992, **87**, 1–22.
4 M. A. McCaffrey, B. Lazar and H. D. Holland, *J. Sediment. Res.*, 1987, **57**, 928–937.
5 J. K. Böhlke and J. J. Irwin, *Geochim. Cosmochim. Acta*, 1992, **56**, 203–225.
6 J. J. Irwin and E. Roedder, *Geochim. Cosmochim. Acta*, 1995, **59**, 295–312.
7 M. Kendrick, R. Duncan and D. Phillips, *Chem. Geol.*, 2006, **235**, 325–351.
8 L.-P. Zeng, X.-F. Zhao, J. Hammerli, T.-W.-T. Fan and C. Spandler, *Miner. Deposita*, 2017, **55**, 1029–1046.
9 D. M. Pyle and T. A. Mather, *Chem. Geol.*, 2009, **263**, 110–121.
10 M. A. Kendrick, M. Honda, T. Pettke, M. Scambelluri, D. Phillips and A. Giuliani, *Earth Planet. Sci. Lett.*, 2013, **365**, 86–96.
11 J. D. Barnes, C. E. Manning, M. Scambelluri and J. Selverstone, in *The Role of Halogens in Terrestrial and Extraterrestrial Geochemical Processes*, ed. D. E. Harlov and L. Aranovich, Springer International Publishing, Cham, 2018, pp. 545–590.
12 M. A. Kendrick and P. Burnard, in *The Noble Gases as Geochemical Tracers*, ed. P. Burnard, Springer, Berlin, Heidelberg, 2013, pp. 319–369.
13 C. Zhu and D. A. Sverjensky, *Geochim. Cosmochim. Acta*, 1992, **56**, 3435–3467.
14 Y. Pan and P. Dong, *Can. Mineral.*, 2003, **41**, 529–540.
15 A. Chan, D. M. Jenkins and M. D. Dyar, *Can. Mineral.*, 2016, **54**, 337–351.
16 H. Li and J. Hermann, *Am. Mineral.*, 2017, **102**, 580–594.
17 E. Hauri, J. Wang, J. E. Dixon, P. L. King, C. Mandeville and S. Newman, *Chem. Geol.*, 2002, **183**, 99–114.
18 E. Hauri, *Chem. Geol.*, 2002, **183**, 115–141.
19 C. Kusebauch, T. John, J. D. Barnes, A. Klugel and H. O. Austrheim, *J. Petrol.*, 2015, **56**, 299–324.
20 C. A. Heinrich, C. G. Ryan, T. P. Mernagh and P. J. Eadington, *Econ. Geol.*, 1992, **87**, 1566–1583.
21 H. Bureau and N. Métrich, *Geochim. Cosmochim. Acta*, 2003, **67**, 1689–1697.
22 J. H. Seo, M. Guillong, M. Aerts, Z. Zajacz and C. A. Heinrich, *Chem. Geol.*, 2011, **284**, 35–44.
23 J. Hammerli, B. Rusk, C. Spandler, P. Emsbo and N. H. S. Oliver, *Chem. Geol.*, 2013, **337–338**, 75–87.
24 C. Zhang, J. Lin, Y. Pan, R. Feng, R. R. Almeev and F. Holtz, *Geostand. Geoanal. Res.*, 2017, **41**, 449–457.
25 S. Flemetakis, J. Berndt, S. Klemme, F. Genske, A. Cadoux, M. Louvel and A. Rohrbach, *Microsc. Microanal.*, 2020, **26**(5), 1076.
26 A. Cadoux, G. Iacono-Marziano, A. Paonita, E. Deloule, A. Aiuppa, G. Nelson Eby, M. Costa, L. Brusca, K. Berlo, K. Geraki, T. A. Mather, D. M. Pyle and I. Di Carlo, *Chem. Geol.*, 2017, **452**, 60–70.
27 M. A. Kendrick, *Chem. Geol.*, 2012, **292–293**, 116–126.
28 J. Hammerli, C. Spandler, N. H. S. Oliver and B. Rusk, *J. Metamorph. Geol.*, 2014, **32**, 93–112.
29 J. J. Donovan and T. N. Tingle, *Microsc. Microanal.*, 1996, **2**, 1–7.
30 C. H. Nielsen and H. Sigurdsson, *Am. Mineral.*, 1981, **66**, 547–552.
31 J. J. Donovan, J. M. Allaz, A. von der Handt, G. G. E. Seward, O. Neill, K. Goemann, J. Chouinard and P. K. Carpenter, *Am. Mineral.*, 2021, **106**, 1717–1735.
32 K. P. Jochum, U. Weis, B. Stoll, D. Kuzmin, Q. Yang, I. Raczek, D. E. Jacob, A. Stracke, K. Birbaum, D. A. Frick, D. Günther and J. Enzweiler, *Geostand. Geoanal. Res.*, 2011, **35**, 397–429.
33 C. Paton, J. Hellstrom, B. Paul, J. Woodhead and J. Hergt, *J. Anal. At. Spectrom.*, 2011, **26**, 2508–2518.
34 T. Pettke, F. Oberli, A. Audétat, M. Guillong, A. C. Simon, J. J. Hanley and L. M. Klemm, *Ore Geol. Rev.*, 2012, **44**, 10–38.
35 M. Kendrick, T. Baker, B. Fu, D. Phillips and P. Williams, *Precambrian Res.*, 2008, **163**, 131–150.
36 R. A. Ketcham, *Am. Mineral.*, 2015, **100**, 1620–1623.
37 M. Louvel, C. Sanchez-Valle, W. J. Malfait, G. S. Pokrovski, C. N. Borca and D. Grolimund, *Solid Earth*, 2020, **11**, 1145–1161.
38 Z. Qiu, H.-R. Fan, A. G. Tomkins, J. Brugger, B. Etschmann, X. Liu, Y. Xing and Y. Hu, *Geochim. Cosmochim. Acta*, 2021, **293**, 256–276.
39 J. T. Nash and J. J. Connor, *Miner. Deposita*, 1993, **28**, 99–106, DOI: 10.1007/BF00196334.
40 M. Gajdošová, M. Huraiova, V. Hurai, M. Slobodnik and P. R. Siegfried, *Acta Geologica Slovaca*, 2019, **11**(2), 63–74.